

Article

The Analysis of Changes in the Crystal Structure of Near-Beta Titanium Alloy in the Solution-Treated and Aged Conditions after Static Tensile Testing

Janusz Krawczyk , Łukasz Frocisz, Marcin Goły , Sylwia Tomasik  and Tomasz Śleboda

Faculty of Metals Engineering and Industrial Computer Science, AGH University of Science and Technology, A. Mickiewicza 30, 30-059 Krakow, Poland; lfrocisz@agh.edu.pl (L.F.); marcing@agh.edu.pl (M.G.); stomasik0@gmail.com (S.T.); sleboda@agh.edu.pl (T.Ś.)

* Correspondence: jkrawcz@agh.edu.pl

Abstract: Titanium alloys are characterized by insufficient ductility. One of the parameters affecting their ductility is their crystal structure and texture. The present study characterizes the changes in the crystallographic texture of the Ti-3Al-8V-6Cr-4Zr-4Mo alloy in solution-treated and aged conditions on the basis of texture intensity indices and pole figures. Analysis of crystal structure changes was performed before and after tensile testing. The investigated alloy in the solution-treated condition showed a single-phase β -solution structure with a body-centered cubic (BCC) crystal structure. The process of β phase aging affected the result of the tensile test, affecting the parameters of the texture of the β phase. The analysis of the texture intensity indices for each set of planes (hkl) related to the intensity for the plane (110) indicated that the highest texture intensity occurs for β titanium alloy aged at 550 °C both before and after tensile test. After plastic deformation, the largest difference with respect to the benchmark value was observed for the (220) and (310) planes. The least amount of texture intensity occurred after aging at 450 °C. The most varied values of diffraction peak intensity in relation to the benchmark were obtained for the alloy aged at 450 °C for the (310), and (200) and (211) planes, indicating the dominance of the (211) orientation, where an elongation of 10.4% was achieved. For the highest elongation of 14.2%, achieved for the sample solution-treated at 550 °C, the diffraction peak intensities were intermediate with the dominance of peaks from the planes (200) and (310).

Keywords: near- β titanium alloy; supersaturation; aging; tensile test; crystallographic texture



Citation: Krawczyk, J.; Frocisz, Ł.; Goły, M.; Tomasik, S.; Śleboda, T. The Analysis of Changes in the Crystal Structure of Near-Beta Titanium Alloy in the Solution-Treated and Aged Conditions after Static Tensile Testing. *Crystals* **2023**, *13*, 1223. <https://doi.org/10.3390/cryst13081223>

Academic Editors: Saif Kayani and Byung Joo Kim

Received: 17 July 2023

Revised: 31 July 2023

Accepted: 4 August 2023

Published: 8 August 2023



Copyright: © 2023 by the authors. Licensee MDPI, Basel, Switzerland. This article is an open access article distributed under the terms and conditions of the Creative Commons Attribution (CC BY) license (<https://creativecommons.org/licenses/by/4.0/>).

1. Introduction

Titanium alloys, due to their unique properties, have found applications in various industries. They are used in the aerospace industry [1], for components for the automotive industry, structural elements in the chemical and petrochemical industries, and for the manufacturing of fasteners [2]. In particular, β titanium alloys compete with the widely used $\alpha + \beta$ alloys due to the possibility to control their properties resulting in their higher strength properties at a lower Young's modulus [3]. Titanium alloys with a body-centered cubic (BCC) crystal structure are characterized by numerous variants of deformation mechanisms. Both dislocation slip, twinning, strain-induced phase transformations and numerous combinations of the above mechanisms are observed. Deformation at the room temperature of a β titanium alloy confirms formation of $\{-1011\}\langle 101-2 \rangle \alpha$ twins. Twinning may occur either through atomic displacement in (1-101) planes along the twinning direction [1-10-2] or due to stress concentration at the α/β interface. Additionally, the formation of the $\{112\}\langle 111 \rangle \beta$ and stress-induced α'' martensitic transformation can be observed. Formation of the twins both in α and β phases can result in the formation of high dislocation density areas, which during further deformation can develop into new grain boundary, promoting the dynamic recrystallization processes. In the case of the quasi-static deformation, the TWIP mechanism can be observed in the metastable titanium alloys. On the other hand, the

increase of strain rate promotes the TRIP effect, essential to maintain the sufficient ductility of titanium alloys [4–12]. Deformation of the near-beta titanium alloys due to their low ductility is mostly performed by hot deformation and the control of the microstructure by continuous recrystallization mechanisms. The continuous formation of new grains during the deformation enables obtaining more complex shapes at higher strain rates during processing. Hot deformation processes of metastable beta titanium alloys at different equivalent strain ranges reveal the strong role of this parameter in the strain hardening of these alloys. High strain rates result in significant strain instability influencing the microstructure. Dynamic recrystallisation is observed in areas of stable deformation, with shear bands mainly observed in areas of higher strain instability. Additionally, dynamic recrystallisation is mostly located at the grain boundaries of the deformed phase, due to the strong accumulation of strain in this area of the material. The energy accumulated in the material provides the driving force for the process of annihilation of linear defects. Continuous dynamic recrystallisation is realized by progressive subgrain rotation, while discontinuous recrystallisation only results in a change in the curvature of the grain boundaries. Continuous recrystallisation processes mainly occur in the material deformed under high strain rates. These processes are related to the dissipation of energy in the material, indicating its correlation to the strain parameters [13–16]. Some researchers point out the main role of dynamic recrystallisation as a factor promoting grain fragmentation in β phase titanium alloys. Dynamic recrystallisation is observed in the areas near the grain boundaries of the β phase. Weakening of the texture intensity in the material associated with this phenomenon was also observed [17–23]. Deformation of titanium alloys below the recrystallization temperature is characterized by the recovery mechanism, while a temperature increase favoring greater mobility of grain boundaries promotes material recrystallisation. The advance of recrystallisation processes also depends on the size of the primary grains in the material before plastic deformation. This is determined by the small number of areas of large change in the crystallographic orientation between grains characteristic of areas of strain inhomogeneity, which is favored by a small amount of grain boundaries. In addition, in the case of the rolling process under larger strains, recrystallisation occurs both at grain boundaries, interfacial boundaries, or inside the grains [24–29]. A non-negligible aspect of the deformation of titanium alloys is the relationship between plastic deformation processes and crystallographic structure. In the case of titanium alloys, it is possible to encounter local perturbations of crystallographic orientation when obtaining a structure that is considered to be mono-dimensional. Certain areas of the material characterized by a distinct crystallographic texture mostly correspond to the orientation of the β phase from which they separated. They preserve the Burgers orientation (BOR) between the grains of the α phase and the β phase in the case of two-phase alloys [30–32]. The occurrence of areas of clearly extreme crystallographic orientation with respect to the rest of the material significantly lowers the material's resistance to fatigue wear [7,33,34]. In titanium alloys, the main crystallographic studies are focused on the study of crystallographic relationships in multiphase systems. The study of deformation of two-phase alloys has indicated that as the strain intensity increases, areas with homogeneous crystallographic orientation are fragmented. In addition, this is positively influenced by intense cooling during heat treatment of these alloys, affecting fragmentation of the original structure before deformation [32]. In contrast, the formation of “<001> and <111> double fiber texture” is observed during the deformation of β titanium alloys [33]. The analysis of changes in the crystallographic structure of near- β titanium alloys is an issue that is still new and requires further research. Hence, this paper focuses on the analysis of changes in the crystallographic structure of near- β titanium alloy under tensile stress and strain during cold deformation. In addition, the effect of heat treatment involving solution treatment and aging on changes in the crystallographic structure of the material, both before and after deformation, was analyzed.

2. Materials and Methods

The test material was a beta C titanium alloy Ti-3Al-8V-6Cr-4Zr-4Mo (designated in the work as TBe). The chemical composition of the alloy is shown in Table 1.

Table 1. The chemical composition of β titanium alloy (wt.%).

| Elements | Al | V | Cr | Zr | Mo |
|-----------------|---------|---------|---------|---------|---------|
| Nominal content | 3.0–4.0 | 7.5–8.5 | 5.5–6.5 | 3.5–4.5 | 3.5–4.5 |
| Actual content | 3.46 | 8.19 | 6.41 | 4.15 | 4.17 |

The tested alloy was subjected to solution treatment at 950 °C for 1 h, and then rapidly cooled in water. Due to the heat treatment, a single-phase microstructure (β phase) was obtained due to the dissolution of the non-equilibrium α phase. The alloy was then subjected to aging at different temperatures. The designations of the test specimens with the corresponding heat treatment parameters are listed in Table 2. The heat treatment was carried out in an FCF 8 M chamber furnace produced by CZYLOK Company (Poland).

Table 2. Heat treatment parameters and the sample notation.

| TBe Alloy Sample | Solution Treatment | Aging |
|------------------|--------------------|------------|
| TBe-S | 950 °C/1 h | - |
| TBe-A450 | 950 °C/1 h | 450 °C/2 h |
| TBe-A500 | 950 °C/1 h | 500 °C/2 h |
| TBe-A550 | 950 °C/1 h | 550 °C/2 h |

The mechanical tests were carried out on 5-fold specimens having rectangular cross-section. The test material was cut by EDM on a wire EDM machine (AG200L, Sodick, Soditronk, Warsaw, Poland) providing precise cutting of any shape. The prepared samples were ground on sandpaper. Cutting the machined material and grinding it allowed to remove microstructural changes in the surface layer of the sample. Static tensile testing was conducted on a Z250 hydraulic press (Zwick/Roell, Wroclaw, Poland). Macroscopic observations of the fracture surfaces were carried out using a Leica Stereozoom S9i microscope (Leica, PIK-Instruments, Piaseczno, Poland).

Diffraction studies were performed on a D8 Advance diffractometer from Bruker corporation using filtered cobalt anode lamp radiation ($\lambda_{\text{CoK}\alpha} = 0.179$ nm). Measurements were performed in the angular range $2\theta = [40\text{--}130^\circ]$ in step mode with a step of $\Delta 2\theta = 0.04^\circ$ and an exposure time per step of 10 s. The phase analysis was performed using PDF (powder diffraction file) patterns from the ICDD (International Center for Diffraction Data) database. A line profile analysis was also carried out. The obtained parameters made it possible to determine texture coefficient (TC), given in Equation (1), which was calculated based on specific intensities of individual diffraction peaks [35]:

$$TC(hkl) = \frac{I(hkl)}{I_0(hkl)} \left\{ \frac{1}{n} \sum \frac{I(hkl)}{I_0(hkl)} \right\}^{-1} \quad (1)$$

where:

I —relative intensity measured for the diffraction line measurement for a given (hkl),
 I_0 —benchmark relative intensity for the diffraction line for a given (hkl) for the non-textured state.

3. Research Results

The static tensile test conducted allowed the determination of parameters such as tensile strength (TS), yield strength (YS) for equal values of elongation, elongation at break (ϵ), yield strength ratio (YS/TS), reduction of area (RA), Young's modulus (E), as well as elastic admissible strain (δ) for individual specimens, all of which are summarized in

Table 3. The elastic admissible strain is defined as the yield strength to Young's modulus ratio ($\delta = YS/E$)

Table 3. Tensile test results for the investigated samples.

| TBe Alloy | TS (MPa) | YS (MPa) | YS/TS (%) | E (GPa) | δ (%) | EL (%) | RA (%) |
|-----------|----------|----------|-----------|---------|--------------|--------|--------|
| TBe-S | 853 | 849 | 99.5 | 182 | 0.47 | 9.9 | 60.2 |
| TBe-A450 | 879 | 873 | 99.3 | 168 | 0.52 | 10.4 | 53.3 |
| TBe-A500 | 869 | 865 | 99.5 | 171 | 0.51 | 9.6 | 43.7 |
| TBe-A550 | 865 | 864 | 99.9 | 163 | 0.53 | 14.2 | 52.9 |

Based on the data shown in Table 3, it can be observed that the tensile strength of the tested materials changes slightly with the aging process of the samples. A slight increase in the value of this parameter can result from the aging process, relative to the solution treated material, with an increase in the aging temperature causing a decrease in the value of tensile strength. A similar relationship can be observed for the yield stress. The yield strength ratio expressed by the YS/TS ratio remains extremely unfavorable. In every case, the value of the yield strength is practically equal to the tensile strength of the material. The aging process of the samples reduced the Young modulus. For β titanium alloy that was not aged, the Young modulus was 181 GPa, while for β titanium alloy aged at 500 °C the Young modulus was 171 GPa, and for β titanium alloy aged at 450 °C the Young modulus value was 168 GPa. The lowest value of 163 GPa was noticed for β titanium alloy aged at 550 °C. A slight increase in the elongation of the sample after the test was also observed. As a consequence of aging, the highest elongation value was obtained for the sample aged at the highest temperature. The values for the solution-treated samples and the samples aged at lower temperatures were similar. The tensile curves obtained during the tests are shown in Figure 1. Three stages of the sample deformation can be observed. Initially, the samples deformed elastically, then after exceeding the yield point, a stage of homogeneous plastic deformation occurred. The last stage involved deformation accompanied by a decrease in stress until rupture. Similar to the data presented in Table 3, it can be observed that the first three samples exhibited a similar character of the flow curve. However, in the case of the sample aged at the highest temperature, the curve showed significantly greater ductility.

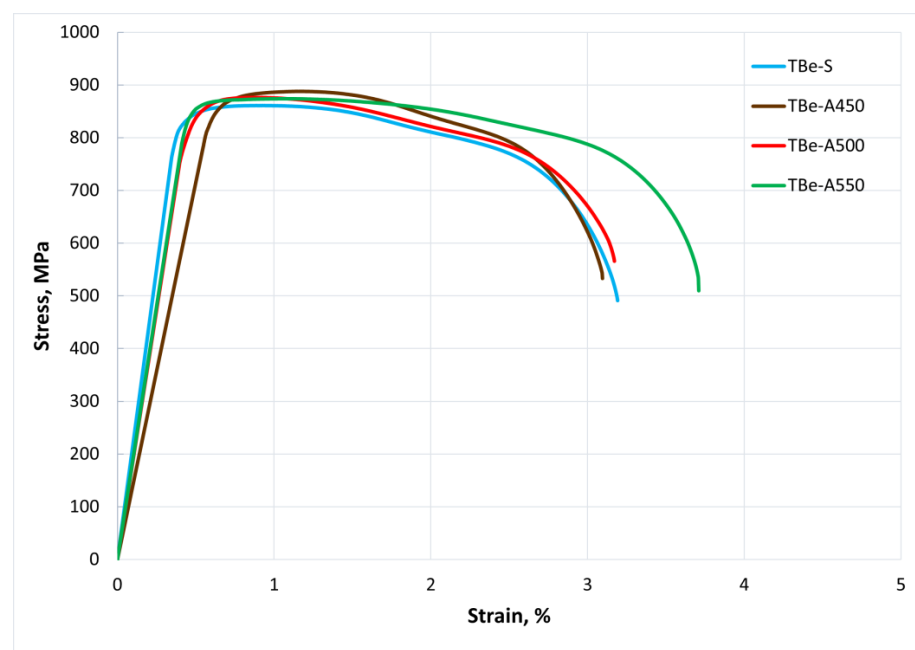


Figure 1. Tensile stress–strain relationship for the investigated alloy.

The next stage of the study was the macroscopic examination of the fractured samples (Figure 2).

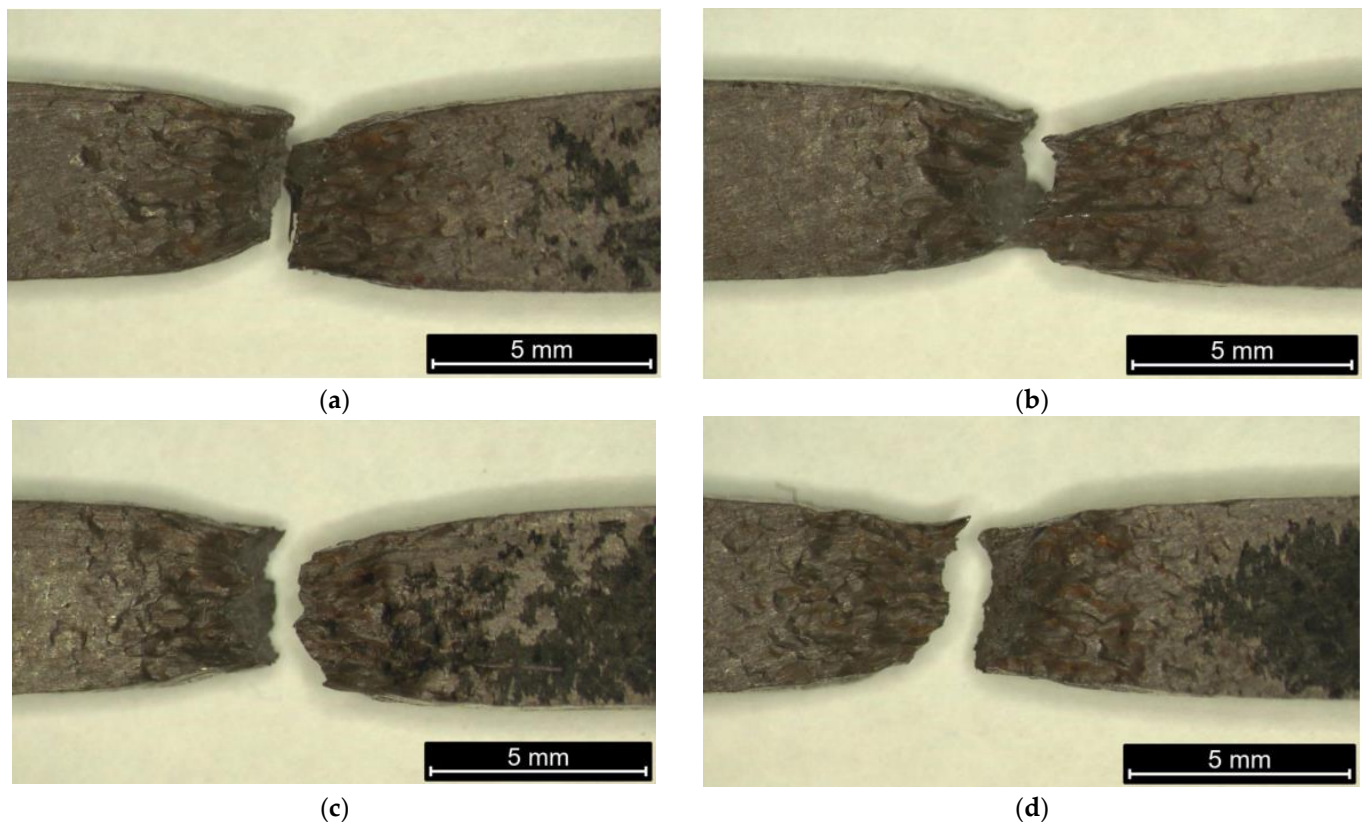


Figure 2. Macroscopic images of the fractured Ti3Al8V6Cr4Zr4Mo alloy samples, (a) after solution treatment at 950 °C/1 h, (b) after solution treatment at 950 °C/1 h and aging at 450 °C/2 h, (c) after solution treatment at 950 °C/1 h and aging at 500 °C/2 h, (d) after solution treatment at 950 °C/1 h and aging at 550 °C/2 h.

It can be observed that there are no significant differences in the fracture surfaces. It can be seen that the sample cross-section reduction and fracture occur fairly parallel on both sides of the samples. Macro images show relief on the surface of the specimen especially in the area of the neck forming. After tensile tests, diffraction studies were performed. The results of X-ray phase analysis of the tested samples are shown in Figure 3.

A slight increase in the intensity of the line (211) for the β phase can be observed as the aging temperature increases. For aging at 550 °C, the peaks from the (220) and (310) planes decrease noticeably. No reflections from the α phase were recorded in any of the analyzed variants. For the reflections from the crystallographic planes observed on the main diffraction lines, the values of TC were determined based on Equation (1). The results of these analyses are shown in Figure 4.

If the TC value significantly deviates from the benchmark value, this allows us to determine which crystallographic planes play a significant role in the deformation process. We can see that the smallest texture was exhibited by β titanium alloy after aging at 450 °C, as indicated by the TC values that were closest to the benchmark value. The largest differences from the benchmark value for β titanium alloy aged at 550 °C (TBe-A550) were noticed. The dominant plane is the (200) plane, with all sets of planes having values greater than the benchmark sample. In the case of the sample aged at 500 °C (TBe-A500), only the reflection from planes (310) showed the highest TC value. On the other hand, as for the reflections from the other planes, they remain at a much lower level than in the case of the benchmark sample (Figure 3a).

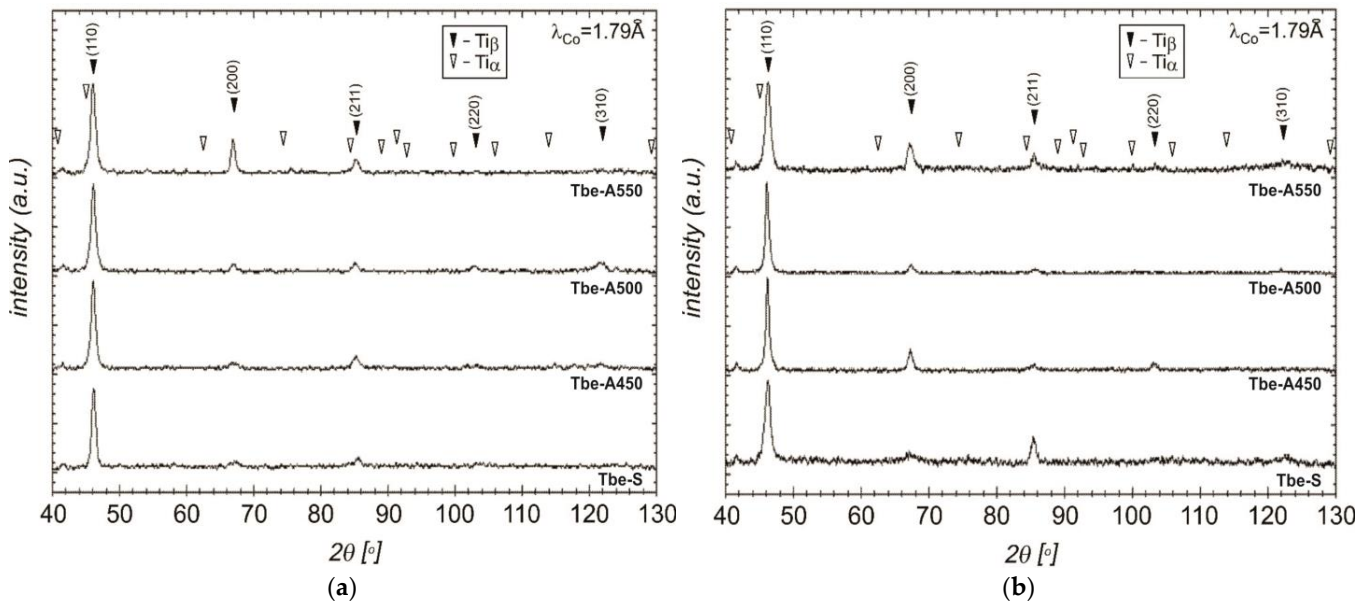


Figure 3. Results of the X-ray diffraction analysis. Phase diffraction patterns for the investigated material after heat treatment: (a) before tensile test, (b) after tensile test.

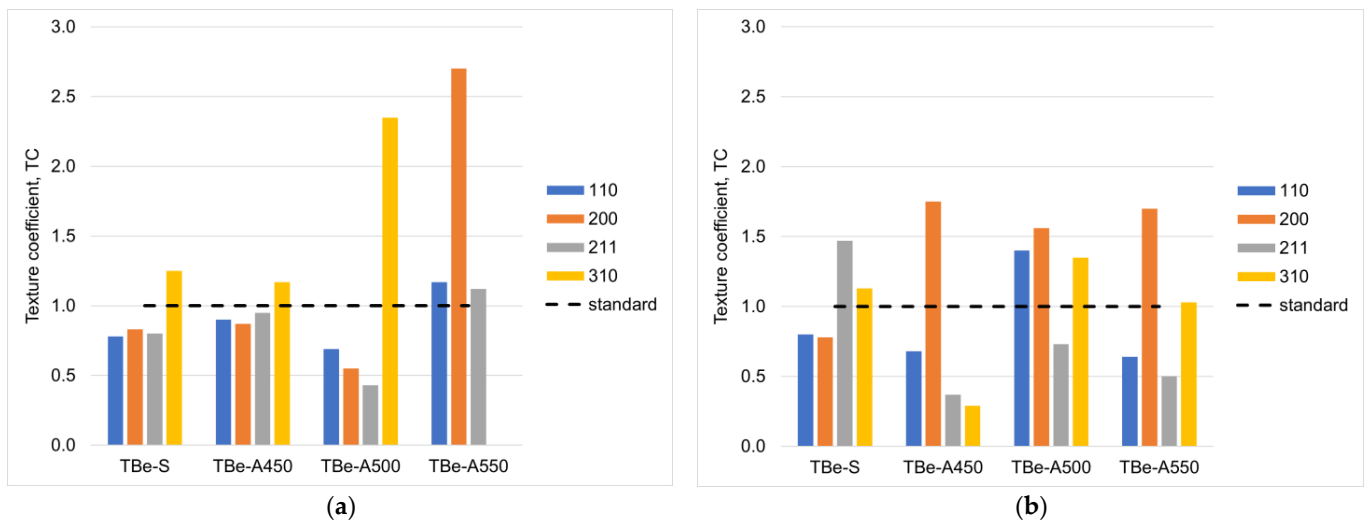
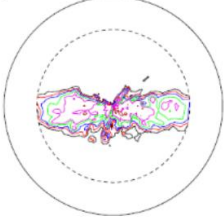
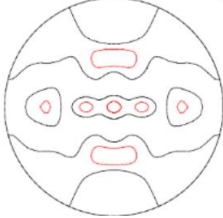
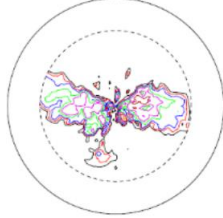
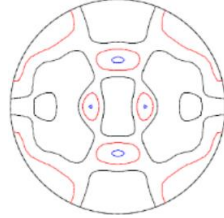
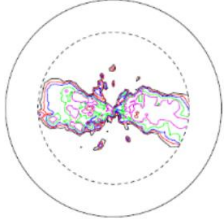
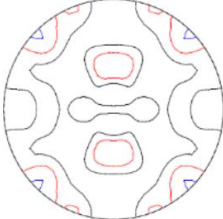
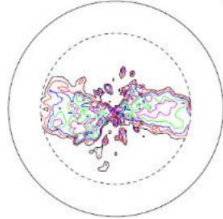
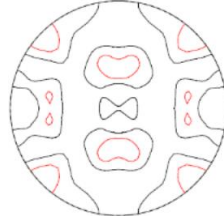
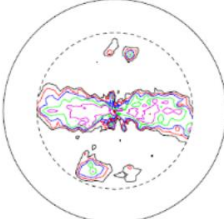
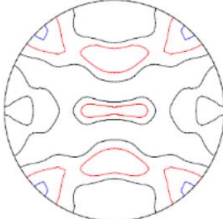
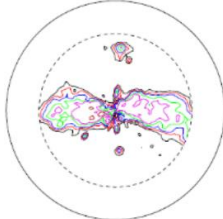
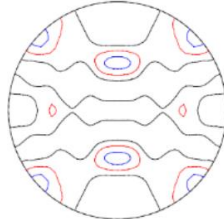
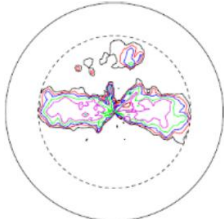
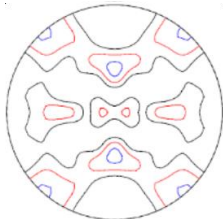
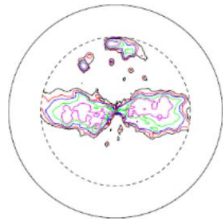
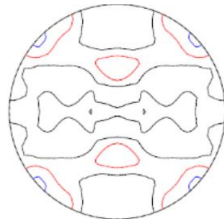


Figure 4. Variation of TC for different diffraction peaks with varied aging temperature (black line signifies TC value for nontextured material): (a) after heat treatment, (b) after heat treatment and tensile test.

After tensile test, an increase in TC values for planes (211) was observed in the case of solution-treated samples. Other values of the TC parameter were similar to those determined before deformation. An increase in the degree of texture intensity was observed for the aged samples. For the lowest aging temperature, a decrease in the degree of texture intensity was observed. Only reflections from planes (200) showed a higher degree of texture intensity. For the aging temperature of 500 °C, the degree of texture intensity increased for all sets of planes. However, for the sample aged at the highest temperature, the texture intensity for the reflections from all planes decreased. Yet, a reflection from a set of planes (310) appeared, which was not observed for the sample before deformation.

In order to illustrate changes in the crystallographic structure of the material as a consequence of deformation processes, it was decided to make polar figures showing changes in the crystallographic texture of the material. The results of this analysis are shown in Table 4.

Table 4. Measured and calculated polar figures for reflection (110) for the test material, rotated by 20°.

| Material Condition | Before Plastic Deformation | | After Plastic Deformation | |
|---|---|---|--|---|
| | Pole Figures | Measured | Calculated | Measured |
| Supersaturation 950 °C/1 h |  |  |  |  |
| Supersaturation 950 °C/1 h Aging 450 °C/2 h |  |  |  |  |
| Supersaturation 950 °C/1 h Aging 500 °C/2 h |  |  |  |  |
| Supersaturation 950 °C/1 h Aging 550 °C/2 h |  |  |  |  |

Polar figures obtained during the test show that the material was only slightly textured after the heat treatment process. The appearance of texture components for the reflection plane (110) was observed especially in the case of the samples aged at the temperatures of 500 °C and 550 °C.

The analysis of the calculated polar figures allowed to indicate greater differences in the texture components. For the (110) plane, a new component enhanced by the aging process became apparent. A similar component remained after deformation of the aged samples. Stronger textures were obtained for the samples aged at 500 °C and 550 °C. Plastic deformation of the solution-treated sample resulted in texture components similar to those obtained for samples aged, undeformed samples.

4. Discussion

The results obtained established that the tested material during cold deformation under tensile stresses was characterized by a very low ratio of yield strength to tensile strength. It can be concluded that the material did not show a range of steady-state flow, where gradual slippage in the material's crystalline structure could occur. In addition, heat treatment showed no significant effect on the strength properties. In the case of this material, the heat treatment did not result in significant changes in the phase composition, and hence the activation of deformation mechanisms associated with sliding along interfacial boundaries or deformation within α phase could be expected [34]. The heat treatment, however, had a significant effect in terms of elastic properties, affecting the reduction of

Young's modulus values. As the aging temperature increased, a gradual decrease in this parameter was observed. This is probably related to the gradual disappearance of the supersaturation of the β phase with alloying elements and the relaxation of stresses in the material, which makes it possible to achieve higher amount of strain in the elastic range. Another important aspect is the increase in sample elongation at the highest aging temperature. It can be supposed that aging at 550 °C resulted in insignificant local increase in grain size. This conjecture coincides with the results of diffraction analysis, where the tested materials for both solution-treated material and the aged material did not show clear texture. However, in the case of aging at 500 °C and 550 °C, higher texture intensity was observed for the (310) and (200) planes, respectively (Figure 3a). Yet, the high values of crystallographic indices for these planes were not conducive to obtaining high strain for this material. The (110)<110> systems supported by slippage along interfacial boundaries are conducive to the high strain values in titanium alloys [36]. No texture oriented in this system was observed in the studied material. On the other hand, after deformation, it was observed that the degree of texture of the material decreased, and the TC value increased mainly for reflections from planes with low texture indices (Figure 3b). However, the small amount of deformation only caused the appearance of new components for planes (110), which confirmed the deformation by sliding along these planes (Figure 4). Nonetheless, high values of tensile stress at low ductility resulted in the activation of deformation mechanisms also in the area of high crystallographic indices, resulting in the appearance of reflections from planes (310) for the material aged at 550 °C also, where previously these reflections were not observed. Strong deformation and the activation of multiple slip systems can also be inferred from the nature of the samples after fracture, where pronounced relief indicates strong deformation and flow of the material, but only in a small volume of the material as the activation of high-index slip systems is associated with strong strain accumulation, without significant deformation of other parts of the material.

Author Contributions: Conceptualization, J.K. and T.Ś.; methodology, M.G., Ł.F. and J.K.; validation, T.Ś. and S.T.; formal analysis, J.K. and Ł.F.; investigation, M.G. and Ł.F.; writing—original draft preparation, Ł.F., T.Ś. and S.T.; writing—review and editing, J.K. and T.Ś. All authors have read and agreed to the published version of the manuscript.

Funding: The research was financed by the Ministry of Education and Science (AGH University of Krakow, the Faculty of Metals Engineering and Industrial Computer Science, research subsidy No. 16.16.110.663, Task No. 18: "Formation of microstructure and properties of beta phase in titanium alloy").

Data Availability Statement: Not applicable.

Acknowledgments: The authors also thank Angelika Dubiel for her support in this research.

Conflicts of Interest: The authors declare no conflict of interest.

References

1. Banerjee, D.; Williams, J.C. Perspectives on Titanium Science and Technology. *Acta Mater.* **2013**, *61*, 844–879. [[CrossRef](#)]
2. Okazaki, Y.; Gotoh, E. Implant Applications of Highly Corrosion-Resistant Ti-15Zr-4Nb-4Ta Alloy. *Mater. Trans.* **2002**, *43*, 2943–2948. [[CrossRef](#)]
3. Wen, M.; Wen, C.; Hodgson, P.; Li, P. Improvement of the biomedical properties of titanium using SMAT and thermal oxidation. *Colloids Surf. B Biointerfaces* **2014**, *116*, 658–665. [[CrossRef](#)]
4. Ahmed, M.; Pereloma, E.V. Observation of simultaneous operation of deformation twins in both α and β phases in metastable β titanium alloy. *J. Alloys Compd.* **2022**, *910*, 164794. [[CrossRef](#)]
5. Zhu, X.; Fan, Q.; Wang, D.; Gong, H.; Gao, Y.; Yuan, J.; Chen, K.; Qian, F. Influence of twins found in adiabatic shear bands on dynamic recrystallization of a near β Ti-5.5Mo-7.2Al-4.5Zr-2.6Sn-2.1Cr alloy. *Mater. Sci. Eng. A* **2022**, *842*, 143084. [[CrossRef](#)]
6. Zhao, Q.; Bolzoni, L.; Chen, Y.; Xu, Y.; Torrens, R.; Yang, F. Processing of metastable beta titanium alloy: Comprehensive study on deformation behaviour and exceptional microstructure variation mechanisms. *J. Mater. Sci. Technol.* **2022**, *126*, 22–43. [[CrossRef](#)]
7. Zhao, J.; Zhong, J.; Yan, F.; Chai, F.; Dargusch, M. Deformation behaviour and mechanisms during hot compression at supertransus temperatures in Ti-10V-2Fe-3Al. *J. Alloys Compd.* **2017**, *710*, 616–627. [[CrossRef](#)]

8. Sinyakova, E.; Panin, A.; Perevalova, O.; Shugurov, A.; Kalashnikov, M.; Teresov, D. The effect of phase transformations on the recovery of pulsed electron beam irradiated Ti-6Al-4V titanium alloy during scratching. *J. Alloys Compd.* **2019**, *795*, 275–283. [[CrossRef](#)]
9. Ellyson, B.; Fezzaa, K.; Sun, T.; Parab, N.; Saville, A.; Finfrock, C.; Rietema, C.; Smith, D.; Copley, J.; Johnson, C.; et al. Transformation and twinning induced plasticity in metastable Ti-Mo alloys under high strain rate deformation. *Mater. Sci. Eng. A* **2022**, *857*, 143716. [[CrossRef](#)]
10. Wu, Z.; Kou, H.; Chen, N.; Zhang, Z.; Qiang, F.; Fan, J.; Tang, B.; Li, J. The effect of cubic-texture on fatigue cracking in a metastable β titanium alloy subjected to high-cycle fatigue. *Int. J. Fatigue* **2020**, *141*, 105872. [[CrossRef](#)]
11. Chen, K.; Fan, Q.; Yang, L.; Yao, J.; Xu, S.; Lei, W.; Gao, Y. Deciphering the microstructural evolution and adiabatic shearing behavior of the titanium alloy with stress-induced ω phase transformation during dynamic compression. *Mater. Des.* **2022**, *221*, 110939. [[CrossRef](#)]
12. Zhang, J.; Qian, B.; Lin, W.; Zhang, P.; Wu, Y.; Fu, Y.; Fan, Y.; Chen, Z.; Cheng, J.; Li, J.; et al. Compressive deformation-induced hierarchical microstructure in a TWIP β Ti-alloy. *J. Mater. Sci. Technol.* **2022**, *112*, 130–137. [[CrossRef](#)]
13. Li, C.; Huang, L.; Zhao, M.; Guo, S.; Li, J. Hot deformation behavior and mechanism of a new metastable β titanium alloy Ti-6Cr-5Mo-5V-4Al in single phase region. *Mater. Sci. Eng. A* **2021**, *814*, 141231. [[CrossRef](#)]
14. Fan, X.; Zhang, Y.; Gao, P.; Lei, Z.; Zhan, M. Deformation behavior and microstructure evolution during hot working of a coarse-grained Ti-5Al-5Mo-5V-3Cr-1Zr titanium alloy in beta phase field. *Mater. Sci. Eng. A* **2017**, *694*, 24–32. [[CrossRef](#)]
15. Chuan, W.; Liang, H. Hot deformation and dynamic recrystallization of a near-beta titanium alloy in the β single phase region. *Vacuum* **2018**, *156*, 384–401. [[CrossRef](#)]
16. Fan, J.; Kou, H.; Lai, M.; Tang, B.; Chang, H.; Li, J. Hot deformation mechanism and microstructure evolution of a new near β titanium alloy. *Mater. Sci. Eng. A* **2013**, *584*, 121–132. [[CrossRef](#)]
17. Lu, T.; Dan, Z.-H.; Li, T.-J.; Dai, G.-Q.; Sun, Y.-Y.; Guo, Y.-H.; Li, K.; Yi, D.-Q.; Chang, H.; Zhou, L. Flow softening and microstructural evolution of near β titanium alloy Ti-35421 during hot compression deformation in the $\alpha+\beta$ region. *J. Mater. Res. Technol.* **2022**, *19*, 2257–2274. [[CrossRef](#)]
18. Matsumoto, H.; Kitamura, M.; Li, Y.; Koizumi, Y.; Chiba, A. Hot forging characteristic of Ti-5Al-5V-5Mo-3Cr alloy with single metastable β microstructure. *Mater. Sci. Eng. A* **2014**, *611*, 337–344. [[CrossRef](#)]
19. Chen, Z.-Q.; Xu, L.-J.; Cao, S.-Z.; Yang, J.-K.; Zheng, Y.-F.; Xiao, S.-L.; Tian, J.; Chen, Y.-Y. Characterization of hot deformation and microstructure evolution of a new metastable β titanium alloy. *Trans. Nonferrous Met. Soc. China* **2022**, *32*, 1513–1529. [[CrossRef](#)]
20. Chen, J.; Li, J.; Tang, B.; Chen, Y.; Kou, H. Microstructure and texture evolution of a near β titanium alloy Ti-7333 during continuous cooling hot deformation. *Prog. Nat. Sci.* **2019**, *29*, 50–56. [[CrossRef](#)]
21. Chen, Y.; Li, J.; Tang, B.; Kou, H.; Xue, X.; Cui, Y. Texture evolution and dynamic recrystallization in a beta titanium alloy during hot-rolling process. *J. Alloys Compd.* **2015**, *618*, 146–152. [[CrossRef](#)]
22. Wang, J.; Wang, K.; Lu, S.; Li, X.; OuYang, D.; Qiu, Q. Softening mechanism and process parameters optimization of Ti-4.2Al-0.005B titanium alloy during hot deformation. *J. Mater. Res. Technol.* **2022**, *17*, 1842–1851. [[CrossRef](#)]
23. Chen, W.; Wang, H.; Lin, Y.C.; Zhang, X.; Chen, C.; Lv, Y.; Zhou, K. The dynamic responses of lamellar and equiaxed near β -Ti alloys subjected to multi-pass cross rolling. *J. Mater. Sci. Technol.* **2020**, *43*, 220–229. [[CrossRef](#)]
24. Chen, W.; Yang, S.; Lin, Y.; Chen, C.; Zhang, X.; Zhou, K. Multi-scale characterization of deformation features and precipitation behavior in a near β -Ti alloy. *Mater. Charact.* **2020**, *169*, 110637. [[CrossRef](#)]
25. Zhu, X.; Fan, Q.; Wang, D.; Gong, H.; Gao, Y.; Qian, F.; Jin, S.; Sha, G. A new dynamic recrystallization mechanism in adiabatic shear band of an α/β dual phase titanium alloy: Composition redistribution. *Scr. Mater.* **2022**, *206*, 114229. [[CrossRef](#)]
26. Furuhashi, T.; Poorganji, B.; Abe, H.; Maki, T. Dynamic recovery and recrystallization in titanium alloys by hot deformation. *JOM* **2007**, *59*, 64–67. [[CrossRef](#)]
27. Ning, Y.; Luo, X.; Liang, H.; Guo, H.; Zhang, J.; Tan, K. Competition between dynamic recovery and recrystallization during hot deformation for TC18 titanium alloy. *Mater. Sci. Eng. A* **2015**, *635*, 77–85. [[CrossRef](#)]
28. Wang, H.; Ge, J.; Zhang, X.; Chen, C.; Zhou, K. Investigation of the Dynamic Recovery and Recrystallization of Near- β Titanium Alloy Ti-55511 during Two-Pass Hot Compression. *Metals* **2021**, *11*, 359. [[CrossRef](#)]
29. Li, J.; Dong, R.; Kou, H.; Fan, J.; Zhu, B.; Tang, B. Texture evolution and the recrystallization behavior in a near β titanium alloy Ti-7333 during the hot-rolling process. *Mater. Charact.* **2020**, *159*, 109999. [[CrossRef](#)]
30. Gu, B.; Chekhonin, P.; Schaarschuch, R.; Oertel, C.-G.; Xin, S.; Ma, C.; Zhou, L.; Gan, W.; Skrotzki, W. Microstructure, texture and hardness of a metastable β -titanium alloy after bar-rolling and annealing. *J. Alloys Compd.* **2020**, *825*, 154082. [[CrossRef](#)]
31. Krawczyk, J.; Tokarski, T.; Łukaszek-Sołek, A.; Dąbrowski, R.; Śleboda, T.; Lypchanskyi, O. Dynamic Recrystallization in Titanium Alloys. *Key Eng. Mater.* **2016**, *687*, 47–54. [[CrossRef](#)]
32. Lypchanskyi, O.; Śleboda, T.; Wojtaszek, M.; Muszka, K.; Łukaszek-Sołek, A.; Stanik, R.; Gude, M. The analysis of flow behavior of Ti-6Al-2Sn-4Zr-6Mo alloy based on the processing maps. *Int. J. Mater. Form.* **2020**, *14*, 523–532. [[CrossRef](#)]
33. Zhang, C.; Jiang, X.; Han, J.; Zhang, S.; Peng, P.; Feng, H.; Wang, T.; Cao, P. Probing the texture transition sequence of near β titanium matrix composites by observing the uneven hot deformation microstructure. *Mater. Charact.* **2023**, *198*, 112728. [[CrossRef](#)]
34. Nasirpour, F.; Sanaeian, M.R.; Samardak, A.S.; Sukovatitsina, E.V.; Ognev, A.V.; Chebotkevich, L.A.; Hosseini, M.-G.; Abdolmaleki, M. An investigation on the effect of surface morphology and crystalline texture on corrosion behavior, structural and magnetic properties of electrodeposited nanocrystalline nickel films. *Appl. Surf. Sci.* **2014**, *292*, 795–805. [[CrossRef](#)]

35. Zhao, Z.B.; Zhang, B.H.; Sun, H.; Wang, Q.J.; Liu, J.R.; Yang, R. Influence of Globularization Process on Local Texture Evolution of a Near- α Titanium Alloy with a Transformed Microstructure. *Metall. Mater. Trans. A* **2014**, *54A*, 2849–2857. [[CrossRef](#)]
36. Du, Z.; Liu, J.; Jiang, S.; Xiao, S.; Kong, F.; Chen, Y. Strain rate dependence of microstructural evolution in β titanium alloy during subtransus superplastic deformation. *J. Alloy. Compd.* **2015**, *647*, 1–5. [[CrossRef](#)]

Disclaimer/Publisher's Note: The statements, opinions and data contained in all publications are solely those of the individual author(s) and contributor(s) and not of MDPI and/or the editor(s). MDPI and/or the editor(s) disclaim responsibility for any injury to people or property resulting from any ideas, methods, instructions or products referred to in the content.